Supporting information

CuAg nanoparticles/carbon aerogel for electrochemical CO_2 reduction

Wenbo Wang[†a], Runqing Lu[†a], Xinxin Xiao[a], Shanhe Gong[a,b], Daniel Kobina Sam[a], Bin Liu[*a], and Xiaomeng Lv[*a]

[a]*School of Chemistry and Chemical Engineering, Jiangsu University, Zhenjiang, 212013, PR China*

[b]*School of the Environment and Safety Engineering, Jiangsu University, Zhenjiang, Jiangsu, 212013, PR China*

Email: liub@ujs.edu.cn (B.Liu) laiyangmeng@163.com(X.M.Lv)

† These authors contributed equally to this paper.

1. Experimental section

1.1 Chemicals and gas

Deionized water was prepared by Jiangsu university. Sodium carbonate (Na_2CO_3, ≥99.5%), Copper nitrate trihydrate ($Cu(NO_3)_2 \cdot 3H_2O$, ≥99%), Silver nitrate ($AgNO_3$, ≥99%), potassium bicarbonate ($KHCO_3$, ≥99.5%), ethanol (CH_3CH_2OH, ≥99.7%), lithium bromide (LiBr, ≥99.5%), N,N-Dimethylformamide (DMF, ≥99.5%) were all purchased from Sinopharm Chemical Reagent Co., Ltd. Cocoon is provided by Institute of Life Sciences, Jiangsu university. Nafion solution (5%) was purchased from Alfa Aesar. High purity carbon dioxide gas (CO_2, 99.99%) and high purity argon (Ar, 99.999%) were purchased from Jiangsu Zhongpu Gas Co., Ltd (China).

1.2 The preparation of silk fibroin (SF) solution

In the typical process, 5 g of silkworm cocoons were dissolved in 0.02 M Na_2CO_3 solution and boiled for 30 min to degumming. The degummed silk was washed with pure water, the SF fiber was dried in an oven at 60 ℃ for 10 h. The degummed silk was then immersed in a 9.5 M LiBr solution to be dissolved to form protein solution at 60 ℃ for 4 h. The protein solution was cooled to room temperature, and dialyzed against pure water for 48 h, then centrifuged at 9000 rpm, and the supernatant was collected and stored at 4 ℃ for further using.

1.3 Electrochemical section

The catalyst ink was dripped on the surface of glassy carbon electrode, and dried to form working electrode at the atmosphere. The working electrode was used to evaluate the double-layer charging (Cdl) of the prepared catalyst at the non-Faraday interval of −0.11 to 0.04 V vs. RHE. which is directly proportional to ECSA of the tested catalyst. The loading of SF-CuAg/CA-N catalyst is 1.43 mg cm^{-2}. The linear sweep voltammetry experiment of SF-CuAg/CA-N catalyst was carried out at the potential rang of 0 to −1.06 V vs. RHE with the scan rate of 5 mV s^{-1}.

The Faradic efficiency (FE) of gas products of online reaction will be calculated by the following formula (Eq. S1)[1]

$$FE_x = \frac{n_x \times F(C/mol) \times V(ml/min) \times 10^{-6}(m^3/ml) \times v(vol\%) \times 1.013 \times 10^5(N/m^2)}{8.314(N \cdot m/mol \cdot K) \times T(K) \times I_{total}(C/s) \times 60(s/min)} \quad \text{(S1)}$$

Where n_x is the number of electrons required to produce a product molecule (H_2, CO = 2, CH_4 =8).

F is the Faradaic constant (96485 C mol^{-1}).

V is the flow rate of CO_2.

v is the volume ratio of gas product obtained from GC data.

The experimental operation was carried out under atmosphere pressure and T of 298.15 K, I_{total} is the cell current of steady-state (C s^{-1}).

The Faradic efficiency (FE) of liquid products was evaluated by the following formula (Eq. S2)[2]

$$FE_x = \frac{n_x ZF}{Q} \quad \text{(S2)}$$

Where n_x is the amount of liquid products,

Z is the number of electrons required to produce a product molecule. Q is total charge during electrocatalysis.

The partial current density of products was obtained according to the formula (Eq. S3)[3]

$$j_x = FE_x \times j_{total} \quad \text{(S3)}$$

Where j_x is the partial current density of product.

j_{total} is the steady-state current density.

1.4 Material characterizations.

Powder XRD patterns of the samples were obtained with an X-ray diffractometer (XRD) (Bruker AXS Company, Germany) equipped with monochromized Cu Kα radiation source (λ=1.54178 Å). X-ray photoelectron spectroscopy (XPS) analysis was obtained using a Thermo Scientific K-Alpha spectrometer equipped with a monochromatic Al Kα radiation source (hv=1486.6 eV, operating voltage: 12 kV). Field emission scanning electron microscope (SEM) images were performed with a field-emission scanning electron microanalyzer (Hitachi S-4800 II, Japan). Transmission electron microscope (TEM, Japan, JEOL-2100F) operated at 100 kV to obtain TEM image of the samples. ^{1}H NMR spectroscopy was performed with a 500

MHz spectrometer (Bruker AVANCE III 500).

2. Supplementary figures

Fig. S1 The physical photograph of the silk fibroin solution

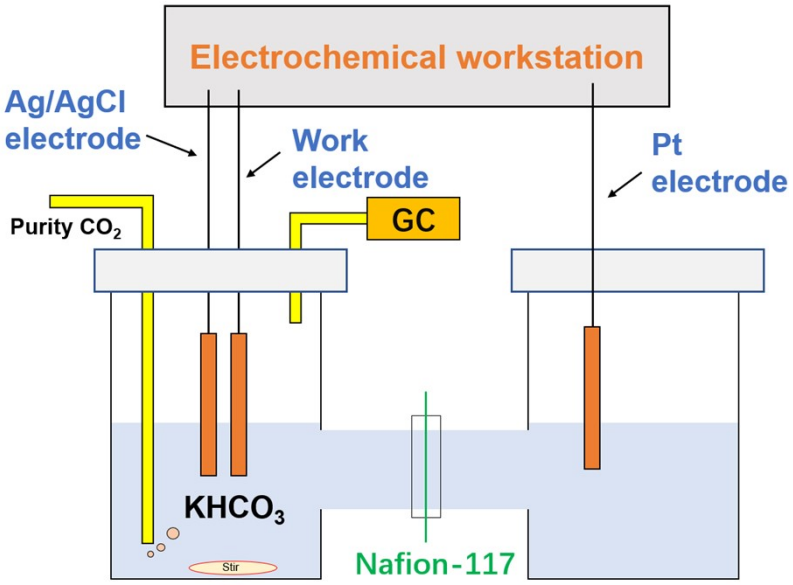

Fig. S2 Schematic illustration of H-type electrolytic cell in this study.

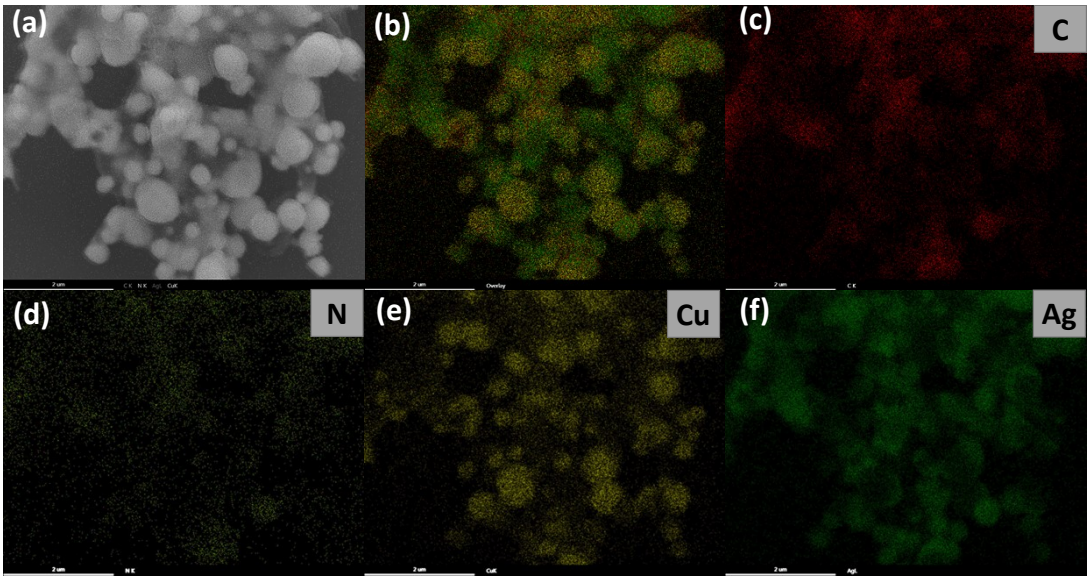

Fig. S3 (a) SEM image of SF-CuAg/CA-40%, element mapping of SF-CuAg/CA-40% (b) overlay，(c) C, (d) N, (e) Cu, (f) Ag, respectively.

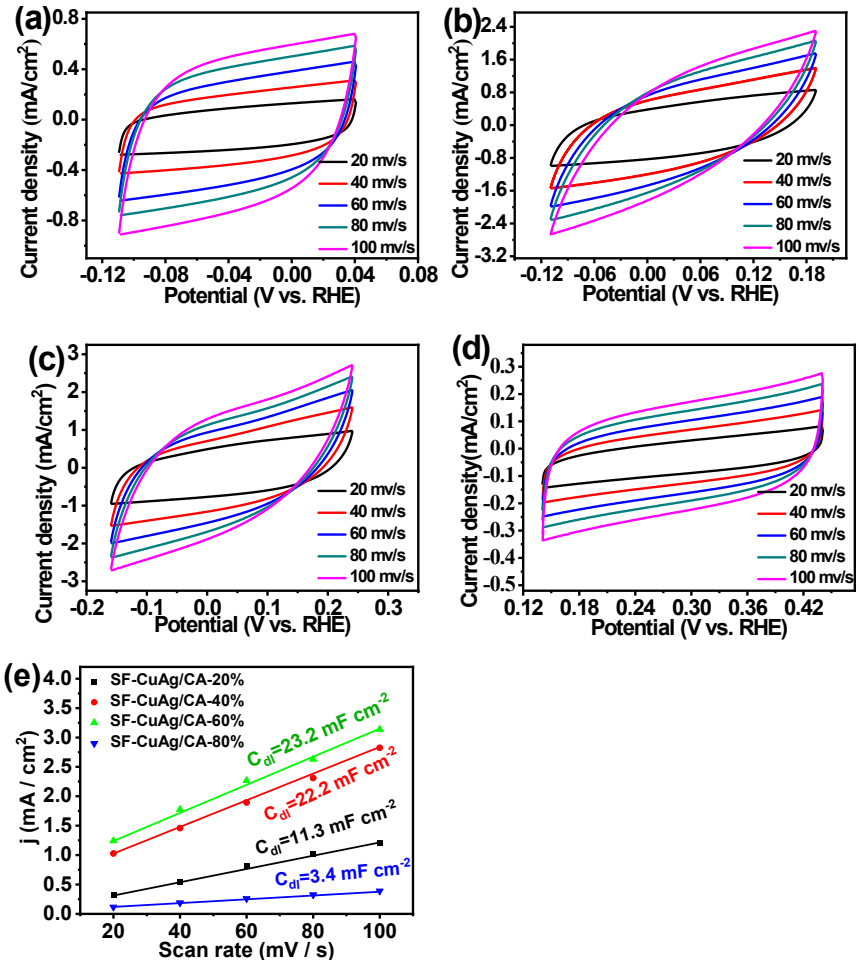

Fig. S4 Cyclic voltammetry curves of SF-CuAg/CA-20% (a), SF-CuAg/CA-40% (b), SF-CuAg/CA-60% (c), SF-CuAg/CA-80% (d). The linear relationship between the current density and the different scan rates (e).

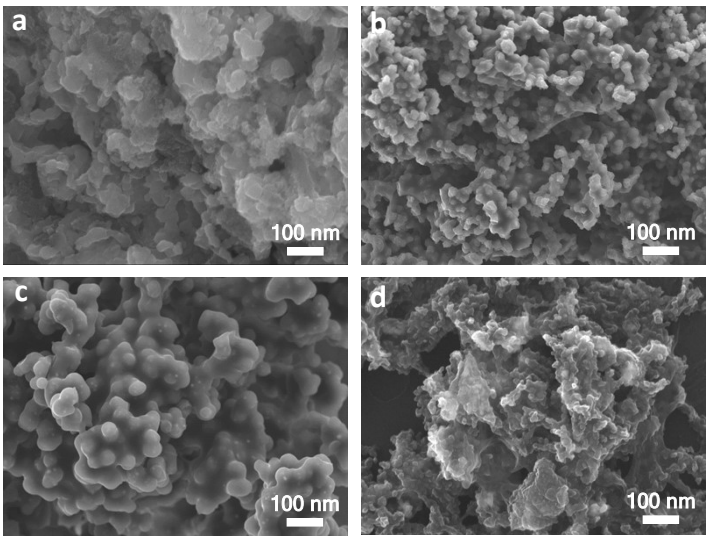

Fig. S5 SEM images of (a) SF-CuAg/CA-20%, (b) SF-CuAg/CA-40%, (c) SF-CuAg/CA-60%, (d)

SF-CuAg/CA-80% after reaction.

3. Supplementary tables

Table S1. XPS analysis results of SF-CuAg/CA-20%, SF-CuAg/CA-40%, SF-CuAg/CA-60% and SF-CuAg/CA-80%.

Samples	C (at%)	O (at%)	N (at%)	Cu (at%)	Ag (at%)
SF-CuAg/CA-20%	74.04%	11.27%	6.91%	4.35%	3.44%
SF-CuAg/CA-40%	74.59%	11.65%	7.09%	5.18%	1.49%
SF-CAAg/CA-60%	73.5%	12.82%	6.98%	5.43%	1.27%
SF-CAAg/CA-80%	75.85%	13.03%	6.95%	3.71%	0.46%

Table S2. ICP analysis results of Ag/Cu atomic ratio of SF-CuAg/CA-20%, SF-CuAg/CA-40%, SF-CuAg/CA-60% and SF-CuAg/CA-80%.

Samples	Ag/Cu (feed ratios)	Ag/Cu (ICP)
SF-CuAg/CA-20%	4:1	3.94:1
SF-CuAg/CA-40%	1.5:1	1.41:1
SF-CuAg/CA-60%	0.67:1	0.67:1
SF-CuAg/CA-80%	0.25:1	0.24:1

Table S3. A comparison of reported Cu-based catalysts for electrochemical CO_2-to-CO conversion in aqueous solution to SF-CuAg/CA-40%.

Catalyst	Electrolyte	Potential	FE_{CO}	J_{CO} (mA cm^{-2})	Stability /potential	Reference
1.9 nm Cu nanoparticles	0.1 M $KHCO_3$	−1.1 V vs. RHE	CO (25%)	−	−	[4]
SF-Cu/CA-1	0.1 M $KHCO_3$	−1.26 V vs. RHE	CO (83.06%)	~29.4	10 h /−1.26 V	[5]
Cu-N_4-C/1100	0.1M phosphate buffer (PBS)+ 0.1M $KHCO_3$	−0.9 V vs. RHE	CO (98%)	~7	40 h /−0.8 V	[6]
Cu–N_2/GN	0.1 M $KHCO_3$	−0.5 V vs. RHE	CO (81%)	~1.62	10 h / −0.5 V	[7]
Ag-Cu bimetallic aerogel	0.1 M $NaHCO_3$	−0.89 V vs. RHE	CO (89.40%)	~5.86	8 h / −0.89 V	[8]
Porous Cu hollow fibres	0.3 M $KHCO_3$	−0.4 V vs. RHE	CO (75%)	~7.50	~0.48 h/−0.4 V	[9]
Cu-In alloy	0.1 M $KHCO_3$	−0.6 V vs. RHE	CO (~88%)	~0.58	~7 h/ −0.6 V	[10]
Cu/CA-CO_2 -N_2 -700	0.1 M $KHCO_3$	−0.6 V vs. RHE	CO (75.6%)	~2.84	10 h /−0.60 V	[11]
Au-Cu	0.5 M $KHCO_3$	−0.91 V vs. RHE	CO (78%)	~46.8	~3 h / −0.91 V	[12]
SF-CuAg/CA-40%	0.1 M $KHCO_3$	−1.26 V vs. RHE	CO (71%)	~15.77 (−1.06 V)	−	This work

4. References

[1] Y. Pan, R. Lin, Y. Chen, S. Liu, W. Zhu, X. Cao, W. Chen, K. Wu, W.C. Cheong, Y. Wang, L. Zheng, J. Luo, Y. Lin, Y. Liu, C. Liu, J. Li, Q. Lu, X. Chen, D. Wang, Q. Peng, C. Chen, Y. Li, J. Am. Chem. Soc. 2018, 140, 4218–4221.

[2] B. Wei, Y. Xiong, Z. Zhang, J. Hao, L. Li, W. Shi, Appl. Catal. B Environ. 2021, 283, 119646.

[3] J. Gu, C.S. Hsu, L. Bai, H.M. Chen, X. Hu, Science 2019, 364, 1091–1094.

[4] R. Reske, H. Mistry, F. Behafarid, B.R. Cuenya, P. Strasser, Particle size effects in the catalytic electroreduction of CO_2 on Cu nanoparticles. J. Am. Chem. Soc. 136 (19) (2014) 6978-6986.

[5] S. H. Gong, X. X. Xiao, W. B. Wang, D. K. Sam, R. Q. Lu, Y. G. Xu, J. Liu, C. D. Wu, X. M. Lv, Silk fibroin-derived carbon aerogels embedded with copper nanoparticles for efficient electrocatalytic CO_2-to-CO conversion, J. Colloid Interf. Sci. 600 (2021) 412-420.

[6] H. Cheng, X. Wu, X. Li, X. Nie, S. Fan, M. Feng, Z. Fan, M. Tan, Y. Chen, G. He, Construction of atomically dispersed Cu-N_4 sites via engineered coordination environment for high-efficient CO_2 electroreduction, Chem. Eng. J. 407 (2021) 126842.

[7] W. Zheng, J. Yang, H. Chen, Y. Hou, Q. Wang, M. Gu, F. He, Y. Xia, Z. Xia, Z. Li, B. Yang, L. Lei, C. Yuan, Q. He, M. Qiu, X. Feng, Atomically defined undercoordinated active sites for highly efficient CO_2 electroreduction, Adv. Funct. Mater. 30 (2020), 1907658.

[8] W. Wang, S. Gong, J. Liu, Y. Ge, J. Wang, X. Lv, Ag-Cu aerogel for electrochemical CO_2 conversion to CO, J. Colloid Interf. Sci. 595 (2021) 159–167.

[9] R. Kas, K.K. Hummadi, R. Kortlever, P. de Wit, A. Milbrat, M.W.J. Luiten-Olieman, N.E. Benes, M.T.M. Koper, G. Mul, Three-dimensional porous hollow fibre copper electrodes for efficient and high-rate electrochemical carbon dioxide reduction, Nat. Commun. 7 (1) (2016) 10748-10754.

[10] S. Rasul, D. H. Anjum, A. Jedidi, Y. Minenkov, L. Cavallo, K. Takanabe, A highly selective copper–indium bimetallic electrocatalyst for the electrochemical reduction of aqueous CO_2 to CO, Angew. Chem. Int. Ed. 127 (7) (2015) 2174-2178.

[11] X. Xiao, Y. Xu, X. Lv, J. Xie, J. Liu, C. Yu, Electrochemical CO_2 reduction on copper nanoparticles-dispersed carbon aerogels, J. Colloid Interf. Sci. 545 (2019) 1-7.

[12] M.K. Birhanu, M.C. Tsai, C. Chen, A.W. Kahsay, T.S. Zeleke, K.B. Ibrahim, C.J. Huang, Y.F. Liao, W. Su, B.J. Hwang, Electrocatalytic reduction of carbon dioxide on gold–copper bimetallic nanoparticles: Effects of surface composition on selectivity, Electrochim. Acta 356 (2020) 136756.